Final Fate of Subcritical Evolutions of Boson Stars

Chi Wai Lai[1, 2, *] and Matthew W. Choptuik[1, 3, 4, †]

[1] *Dept. of Physics and Astronomy, University of British Columbia, Vancouver BC, V6T 1Z1 Canada*
[2] *Dept. of Physics, The Hong Kong University of Science and Technology, Clear Water Bay, Kowloon, Hong Kong*
[3] *CIFAR Cosmology and Gravity Program*
[4] *Max-Planck-Institut für Gravitationsphysic, Albert-Einstein-Institut, Am Mühlenberg 1, D-14476 Golm, Germany*

We present results from a study of Type I critical phenomena in the dynamics of general relativistic boson stars in spherical symmetry. The boson stars are modelled with a minimally coupled, massive complex field (with no explicit self-interaction), and are driven to the threshold of black hole formation via their gravitational interaction with an initially imploding pulse of massless scalar field. Using a distinct coordinate system, we reproduce previous results [1, 2], including the scaling of the lifetime of near-critical configurations, as well as the fact that such configurations are well described as perturbed, one-mode-unstable boson stars. In addition, we make a detailed study of the long-time evolution of marginally subcritical configurations. Contrary to previous claims [1, 2], we find that the end state in such cases does not involve dispersal of the bulk of the boson star field to large radial distances, but instead can be generically described by a stable boson star executing large amplitude oscillations. Furthermore we show that these oscillations can be largely identified as excitations of the fundamental mode associated with the final boson star, as computed in perturbation theory.

I. INTRODUCTION

Over the past decade or so, intricate and unexpected phenomena related to black holes have been discovered through the detailed numerical study of various models for gravitational collapse, starting with one of the authors' investigation of the spherically symmetric collapse of a massless scalar field [3]. These studies generally concern the *threshold* of black hole formation (a concept described below), and the phenomena observed near threshold are collectively called (black hole) critical phenomena, since they share many of the features associated with critical phenomena in statistical mechanical systems. The study of critical phenomena continues to be an active area of research in numerical relativity, and we refer the interested reader to the review article by Gundlach [4] for full details on the subject. Here we will simply summarize some key points that are most germane to the work described in this paper.

To understand black hole critical phenomena, one must understand the notion of the "threshold of black hole formation". The basic idea is to consider *families* of solutions of the coupled dynamical equations for the gravitational field and the matter field that is undergoing collapse (a complex scalar field, ϕ, in our case). Since we are considering a dynamical problem, and since we assume that the overall dynamics is uniquely determined by the initial conditions, we can view the families as being parametrized by the initial conditions—variations in one or more of the parameters that fix the initial values will then generate various solution families. We also emphasize that we are considering collapse problems. This

means that we will generically be studying the dynamics of systems that have length scales comparable to their Schwarzschild radii, *for at least some period of time during the dynamical evolution*. We also note that we will often take advantage of the complete freedom we have as numerical experimentalists to choose initial conditions that lead to collapse, but which may be highly unlikely to occur in an astrophysical setting.

We now focus attention on single parameter families of data, so that the specification of the initial data is fixed up to the value of *the* family parameter, p. We will generally view p as a non-linear control parameter that will be used to govern how strong the gravitational field becomes in the subsequent evolution of the initial data, and in particular, whether a black hole forms or not. Specifically, we will always demand that any one-parameter family of solutions has the following properties:

1. For sufficiently small values of p the dynamics remain regular for all time, and no black hole forms.

2. For sufficiently large values of p, complete gravitational collapse sets in at some point during the dynamical development of the initial data, and a black hole forms.

From the point of view of simulation, it turns out to be a relatively easy task for many models of collapse to construct such families, and then to identify two specific parameter values, p^- (p^+) which do not (do) lead to black hole formation. Once such a "bracket" $[p^-, p^+]$ has been found, it is straightforward in principle to use a technique such as binary search to hone in on a *critical parameter value*, $p^\star$, such that all solutions with $p < p^\star$ ($p > p^\star$) do not (do) contain black holes. A solution corresponding to $p = p^\star$ thus sits at the threshold of black hole formation, and is known as a *critical solution*. It should be emphasized that underlying the existence of critical solutions are the facts that (1) the end states (infinite-time

behaviour) corresponding to properties 1 and 2 above are *distinct* (a spacetime containing a black hole *vs* a spacetime not containing a black hole) and (2) the process characterizing the black hole threshold (i.e. gravitational collapse) is *unstable*. We also note that we will term evolutions with $p < p^\star$ *subcritical*, while those with $p > p^\star$ will be called *supercritical*.

Having discussed the basic concepts underlying black hole critical phenomena, we now briefly describe the features of critical collapse that are most relevant to the research described below.

First, critical solutions *do* exist for all matter models that have been studied to date, and for any given matter model, almost certainly constitute discrete sets. In fact, for some models, there may be only *one* critical solution, and we therefore have a form of universality.

Second, critical solutions tend to have additional symmetry beyond that which has been adopted in the specification of the model (e.g. we will impose spherical symmetry in our calculations).

Third, the critical solutions known thus far, and the black hole thresholds associated with them, come in two broad classes. The first, dubbed Type I, is characterized by static or periodic critical solutions (i.e. the additional symmetry is a continuous or discrete time-translational symmetry), and by the fact that the black hole mass just above threshold is *finite* (i.e. so that there is a minimum black hole mass that can be formed from the collapse). The second class, called Type II, is characterized by continuously or discretely self-similar critical solutions (i.e. the additional symmetry is a continuous or discrete scaling symmetry), and by the fact that the black hole mass just above threshold is *infinitesimal* (i.e. so that there is *no* minimum for the black hole mass that can be formed). The nomenclature Type I and Type II is by analogy with first and second order phase transitions in statistical mechanics, with the black hole mass viewed as an order parameter.

Fourth, solutions close to criticality exhibit various scaling laws. For example, in the case of Type I collapse, where the critical solution is an unstable, time-independent (or periodic) compact object, the amount of time, τ, that the dynamically evolved configuration is well approximated by the critical solution *per se* satisfies a scaling law of the form

$$\tau(p) \sim -\gamma \ln |p - p^\star| \,, \qquad (1)$$

where γ is a *universal* exponent in the sense of not depending on which particular family of initial data is used to generate the critical solution, and $\sim$ indicates that the relation (1) is expected to hold in the limit $p \to p^\star$.

Fifth, and finally, much insight into critical phenomena comes from the observation that although unstable, critical solutions tend to be *minimally* unstable, in the sense that they tend to have only a few, and perhaps only one, unstable modes in perturbation theory. In fact, if one assumes that a Type I solution, for example, has only a single unstable mode, then the growth factor (Lyapunov exponent) associated with that mode can be immediately related to the scaling exponent γ defined by (1).

In this paper we will be exclusively concerned with Type I critical phenomena, where the threshold solutions will generally turn out to be unstable boson stars. Previous work relevant to ours includes studies by Hawley [1] and Hawley & Choptuik [2] of boson stars in spherically symmetry. We extend this work and show that, contrary to previous claims [1, 2] that subcritical solutions disperse most of the original mass of the boson star to large distances—the late time behaviour of subcritical evolution is characterized by oscillation about a stable boson star solution. We also apply a linear perturbation analysis similar to that in [1, 2] and confirm that the observed oscillation modes agree with the fundamental modes given by perturbation theory. (We use a code kindly provided by S. Hawley [5] to generate the frequencies from the perturbation analysis.)

The outline of the rest of this paper is as follows: in Section II we describe the mathematical formulation for our numerical simulations, which includes II A: the model for the boson stars, and II B: the initial value problem. In Section III we present results of our simulations: in III A we present the setup of numerical experiments, in III B the Type I character of the critical solutions is demonstrated, III C contains a discussion of the end state of subcritical evolutions and is followed by some perturbation analysis in III D. Section IV summarizes our findings, while the finite difference approximations used and our convergence testing of our implementations of them, are given in Appendices A and B respectively.

In what follows we base our work in the context of classical field theory, and we choose units in which $G = c = 1$. In addition, without loss of generality, we restrict ourselves to the case where the particle mass, m, associated with the complex scalar field satisfies $m = 1$.

II. MATHEMATICAL FORMULATION

A. The model

Our model for boson stars involves a self-gravitating massive complex scalar field, $\phi = \phi_1 + i\phi_2$, minimally coupled to gravity as given by general relativity. (Note that we do not make the complex scalar field explicitly self-interacting—in the literature, the stationary configurations in this case are sometimes called "mini" boson stars.) An additional, massless real scalar field, ϕ_3, also minimally coupled to gravity, is used to dynamically "perturb" the boson star. The interaction between the massive complex scalar field and the massless real scalar field is thus through the gravitational field alone. The whole system can be described by the action

$$S = \int d^4 x \sqrt{-g} \left[\frac{R}{16\pi} - \frac{1}{2} \left(\nabla^\mu \phi \nabla_\mu \phi^* + m^2 \phi \phi^* \right) - \frac{1}{2} \nabla^\mu \phi_3 \nabla_\mu \phi_3 \right] , \qquad (2)$$

where R is the spacetime Ricci scalar and m is the mass of the bosonic particle. Variations of the action with respect to the metric, $g_{\mu\nu}$, the complex scalar field, ϕ, and the real scalar field, ϕ_3, yield the equations of motion, which are the Einstein equation, the Klein-Gordon equation and the wave equation, respectively:

$$R_{\mu\nu} - \frac{1}{2} g_{\mu\nu} R = 8\pi T_{\mu\nu} , \qquad (3)$$

$$\nabla^\mu \nabla_\mu \phi - m^2 \phi = 0 , \qquad (4)$$

and

$$\nabla^\mu \nabla_\mu \phi_3 = 0 , \qquad (5)$$

where

$$T_{\mu\nu} = T_{\mu\nu}^\phi + T_{\mu\nu}^{\phi_3} , \qquad (6)$$

$$T_{\mu\nu}^\phi \equiv \frac{1}{2} \left[(\nabla_\mu \phi \nabla_\nu \phi^* + \nabla_\nu \phi \nabla_\mu \phi^*) - g_{\mu\nu} \left(\nabla^\alpha \phi \nabla_\alpha \phi^* + m^2 |\phi|^2 \right) \right] , \qquad (7)$$

$$T_{\mu\nu}^{\phi_3} = \nabla_\mu \phi_3 \nabla_\nu \phi_3 - \frac{1}{2} g_{\mu\nu} \nabla^\alpha \phi_3 \nabla_\alpha \phi_3 . \qquad (8)$$

Equations (3)–(8) completely determine the dynamics of our system (up to coordinate transformations), once appropriate initial conditions and boundary conditions are specified.

To study the system numerically, we adopt the standard "3+1" ADM formalism [6, 7]. Since we restrict ourselves to spherically symmetry the metric can be written in a much simpler form than in the generic case. Here we use maximal-isotropic coordinates, which is a different system than that used in [1, 2]. We note in passing that although the accuracy of finite difference calculations in any given coordinate system can in principle be estimated using intrinsic means (e.g. convergence tests), we feel that it is nonetheless useful to reproduce the calculations of [1, 2] in a distinct coordinate system.

In maximal-isotropic coordinates, the line element can be written as:

$$ds^2 = \left(-\alpha^2 + \psi^4 \beta^2 \right) dt^2 + 2\psi^4 \beta \, dt \, dr + \psi^4 \left(dr^2 + r^2 d\Omega^2 \right) , \quad (9)$$

where α, β and ψ are the lapse function, r-component of the shift vector and the conformal factor respectively, and all are functions of t and r. We further define new variables to transform the Klein Gordon and wave equations into a first order (in time) system:

$$\Phi_i \equiv \phi_i' , \qquad (10)$$

$$\Pi_i \equiv \frac{\psi^2}{\alpha} \left(\dot\phi_i - \beta \phi_i' \right) , \qquad (11)$$

where $i = 1, 2$ or 3, $' \equiv \partial/\partial r$ and $\dot{} \equiv \partial/\partial t$. As with the geometric variables, ϕ_i. Φ_i and Π_i are functions of t and r alone.

With these definitions, the Hamiltonian constraint and momentum constraints are given by [8]

$$\frac{3}{\psi^5} \frac{d}{dr^3} \left(r^2 \frac{d\psi}{dr} \right) + \frac{3}{16} K^r{}_r{}^2 = - \pi \left(\frac{\sum_{i=1}^3 \left(\Phi_i^2 + \Pi_i^2 \right)}{\psi^4} + m^2 \sum_{i=1}^2 \phi_i{}^2 \right), (12)$$

$$K^r{}_r{}' + 3 \frac{(r\psi^2)'}{r\psi^2} K^r{}_r = -\frac{8\pi}{\psi^2} \left(\sum_{i=1}^3 \Pi_i \Phi_i \right) , \qquad (13)$$

and the Klein-Gordon and wave equations become

$$\dot\phi_i = \frac{\alpha}{\psi^2} \Pi_i + \beta \Phi_i , \qquad (14)$$

$$\dot\Phi_i = \left(\beta \Phi_i + \frac{\alpha}{\psi^2} \Pi_i \right)' , \qquad (15)$$

$$\dot\Pi_i = \frac{3}{\psi^4} \frac{d}{dr^3} \left[r^2 \psi^4 \left(\beta \Pi_i + \frac{\alpha}{\psi^2} \Phi_i \right) \right] - \alpha \psi^2 m^2 \phi_i (1 - \delta_{i3}) - \left(\alpha K^r{}_r + 2\beta \frac{(r\psi^2)'}{r\psi^2} \right) \Pi_i . \qquad (16)$$

In addition to equations (12)–(16), we need to determine the lapse function and shift component using our specific coordinate choices. The maximal condition, which maximizes the 3-volume of the $t = $ const. slices, is given by $K \equiv K^i{}_i = 0$. This is implemented by choosing initial data so that $K(0, r) \equiv 0$ and then demanding that

$$\dot K(t, r) = 0 . \qquad (17)$$

for all t and r.

This leads to the following linear ODE for $\alpha(t,r)$, which must be solved at each instant in time in order to maintain the maximal condition [8]:

$$\alpha'' + \frac{2}{r\psi^2}\frac{d}{dr^2}\left(r^2\psi^2\right)\alpha'$$
$$+ \left(4\pi m^2\psi^4\sum_{i=1}^{2}\phi_i^2 - 8\pi\sum_{i=1}^{3}\Pi_i^2 - \frac{3}{2}(\psi^2 K^r{}_r)^2\right)\alpha$$
$$= 0. \qquad (18)$$

The isotropic condition, which is implicit in the chosen form of the metric (9), demands that the 3-metric of each $t = \mathrm{const.}$ hypersurface be conformally flat. This requirement leads to the following ODE for the shift vector component, $\beta(t,r)$:

$$r\left(\frac{\beta}{r}\right)' = \frac{3}{2}\alpha K^r{}_r. \qquad (19)$$

Equations (12)–(19) constitute a complete set of differential equations governing our model. Note that our approach is an instance of so-called fully constrained evolution, wherein all of the geometric variables—ψ and $K^r{}_r$ in this case—are computed at each time step using constraint equations. To completely fix a solution—given initial data—we also must impose regularity and boundary conditions at $r = 0$ and $r \to \infty$ respectively.

Regularity at the origin, $r = 0$, requires

$$\psi'(t,0) = 0, \qquad (20)$$
$$K^r{}_r(t,0) = 0, \qquad (21)$$
$$\alpha'(t,0) = 0, \qquad (22)$$
$$\phi_i'(t,0) = 0, \qquad (23)$$
$$\Pi_i'(t,0) = 0, \qquad (24)$$

whereas the outer boundary conditions are

$$\lim_{r\to\infty}\psi(t,r) = 1 + \frac{C(t)}{r} + O(r^{-2}), \qquad (25)$$

$$\lim_{r\to\infty}\alpha(t,r) = \lim_{r\to\infty}\frac{2}{\psi(t,r)} - 1$$
$$= 1 - \frac{2C(t)}{r} + O(r^{-2}), \qquad (26)$$

$$\lim_{r\to\infty}\beta(t,r) = \frac{D(t)}{r} + O(r^{-2}), \qquad (27)$$

and

$$\dot{\Phi}_i + \Phi_i' + \frac{\Phi_i}{r} = 0, \qquad (28)$$

$$\dot{\Pi}_i + \Pi_i' + \frac{\Pi_i}{r} = 0, \qquad (29)$$

for some functions $C(t)$ and $D(t)$. The last two of these equations are approximate Sommerfeld conditions that assume that as $r \to \infty$, the three scalar field components, ϕ_i, are purely outgoing with amplitudes decaying as $1/r$. For given initial data, eqs. (12)–(29) now completely determine our system.

For diagnostic purposes, we also define the mass aspect function

$$M(t,r) \equiv \left(\frac{\psi^2 r}{2}\right)^3 K^r{}_r{}^2 - 2\psi'r^2\left(\psi + r\psi'\right), \qquad (30)$$

which is equal to the ADM mass in any vacuum region exterior to the support of matter.

In addition, although ψ and $K^r{}_r$ are ultimately determined from the constraint equations, the following evolution equations are used for providing initial estimates for the iterative constraint-solving process.

$$\dot{\psi} = -\frac{1}{2}\alpha\psi K^r{}_r + \frac{(\psi^2\beta)'}{2\psi}, \qquad (31)$$

$$\dot{K^r{}_r} = \beta K^{r\prime}{}_r - \frac{2\alpha}{(r\psi^2)^2} + \frac{2}{r^2\psi^6}\left[\alpha r\left(r\psi^2\right)'\right]'$$
$$+ 8\pi m^2\alpha|\phi|^2. \qquad (32)$$

Full details of our finite differencing scheme are given in App. A.

B.   The initial value problem

The primitive object in our model problem is a (ground-state) boson star, represented by a configuration of massive complex scalar field, centred at the origin. Ideally one would like a "star" to be described by a localized, time-independent matter source that generates an everywhere regular (i.e. non-singular) gravitational field. However, for the case of a complex scalar field, it can be shown that such regular, time-independent configurations do not exist [9]. Despite this fact, since the stress-energy tensor (7) depends only on the modulus of the scalar field (and the gradients of the modulus), one *can* construct scalar field configurations with harmonic time-dependence that produce time-independent metrics. Specifically, we adopt the following ansatz for boson stars in spherical symmetry:

$$\phi(t, r) = \phi_0(r)\, e^{-i\omega t}\,, \qquad (33)$$

and then demand that the spacetime be static, i.e. we demand that the metric admits a timelike Killing vector field, χ, which is orthogonal to the $t = $ const. surfaces. Adapting coordinate time to the timelike Killing vector field, we have

$$\beta = 0\,, \qquad (34)$$

for all time t. Additionally, we have that the time derivatives of any of the geometrical variables identically vanish. It then follows immediately that [8]

$$K^r{}_r = 0\,. \qquad (35)$$

As is necessary for the consistency of the ansatz (33), the isotropic condition for β (19) is automatically satisfied, and we are left with geometrical variables $\alpha(0, r)$, $\psi(0, r)$ and $\phi_0(r)$ that need to be determined from the maximal slicing condition (18), the Hamiltonian constraint (12) and the Klein-Gordon equation (16), respectively:

$$\psi' = \Psi\,, \qquad (36)$$
$$\Psi' = -\frac{2\Psi}{r} - \pi\left[\psi\Phi^2 + \psi^5\left(\frac{\omega^2}{\alpha^2} + m^2\right)\phi^2\right]\,, \quad (37)$$
$$\phi' = \Phi\,, \qquad (38)$$
$$\Phi' = -\left(\frac{2}{r} + \frac{A}{\alpha} + \frac{2\Psi}{\psi}\right)\Phi + \psi^4\left(m^2 - \frac{\omega^2}{\alpha^2}\right)\phi\,, (39)$$
$$\alpha' = A\,, \qquad (40)$$
$$A' = -2\left(\frac{1}{r} + \frac{\Psi}{\psi}\right)A + 4\pi\psi^4\alpha\left(\frac{2\omega^2}{\alpha^2} - m^2\right)\phi^2 (41)$$

Here, in order to simplify notation, we have dropped the subscript "0", making the identifications $\phi(r) \equiv \phi_0(r)$ and $\Phi(r) \equiv \phi'(r) \equiv \phi_0'(r)$. We have also introduced auxiliary variables $\Psi(r) \equiv \psi'(r)$ and $A(r) \equiv \alpha'(r)$ in order to cast the above system of nonlinear ODEs in a canonical first-order form. We assert that for any given value of $\phi(0) \equiv \phi_0(0)$, the system (36)-(41) constitutes an eigenvalue problem with eigenvalue $\omega = \omega(\phi(0))$. That is, for any specific value of $\phi(0)$ (which one can loosely view as being related to the central density of the star), a solution of (33) that satisfies the appropriate regularity and boundary conditions will only exist for some specific value of ω. The system (36)–(41) must be supplemented by boundary conditions, some of which are naturally applied at $r = 0$, with the rest naturally set at $r = \infty$. In particular, regularity at $r = 0$ implies

$$\Psi(0) = 0\,, \qquad (42)$$
$$\Phi(0) = 0\,, \qquad (43)$$
$$A(0) = 0\,, \qquad (44)$$

while at the outer boundary, we have

$$\lim_{r\to\infty} \psi(r) = 1 - \frac{C}{r}\,, \qquad (45)$$
$$\lim_{r\to\infty} \phi(r) \approx 0\,, \qquad (46)$$
$$\lim_{r\to\infty} \alpha(r) = \frac{2}{\psi} - 1\,. \qquad (47)$$

Here the second condition follows from the expectation that ϕ should decay exponentially [10] as $r \to 0$.

We further note that due to the homogeneity and linearity of the slicing equation, we can always arbitrarily (and conveniently) choose the central value of the lapse via

$$\alpha(0) = 1\,, \qquad (48)$$

and then, after integration of (36)-(41), can rescale α and ω simultaneously to satisfy the true outer boundary condition, (47), for α:

$$\alpha(r) \longrightarrow c\,\alpha(r)\,, \qquad (49)$$
$$\omega(r) \longrightarrow c\,\omega(r)\,. \qquad (50)$$

where c is given by

$$c = \frac{2/\psi(r_{\max}) - 1}{\alpha(r_{\max})}\,, \qquad (51)$$

and $r_{\max}$ is the radial coordinate of the outer boundary of the computational domain.

As mentioned above, any solution of (36)-(41) can be conveniently labelled by the central value of the modulus of the scalar field, $\phi_0(0) = \phi(0)$. For any given value of $\phi_0(0)$, we must then determine the eigenvalue, ω, and in the current case of maximal-isotropic coordinates, the central value of the conformal factor $\psi(0)$, so that all of the boundary conditions are satisfied. In principle, we can compute pairs $[\omega, \psi(0)]$ as a function of $\phi_0(0)$ using a two-parameter "shooting" technique [11, 12].

Alternatively, in some cases we generate boson star initial data in maximal-isotropic coordinates by first constructing the stars in so-called polar-areal coordinates, and then performing a coordinate transformation on the resulting solution.

Polar-areal coordinates, which have seen widespread use in spherically symmetric computations in numerical relativity, can be viewed as the generalization of the usual Schwarzschild coordinates to *time-dependent*, spherically symmetric spacetimes. As with maximal slicing, the slicing condition in this case—known as polar slicing—is expressed as a condition on the mean extrinsic curvature:

$$K = K^r{}_r\,. \qquad (52)$$

Since in general we have $K = K^i{}_i = K^r{}_r + 2K^\theta{}_\theta$, this condition is implemented by requiring

$$K^\theta{}_\theta(t, r) = \dot{K}^\theta{}_\theta(t, r) = 0\,, \qquad (53)$$

for all t and r.

The spatial coordinates are fixed by demanding that the coordinate r measure proper surface area (i.e. that it be an *areal* coordinate). It can be shown that this choice of r, together with polar slicing, further imply that $\beta \equiv 0$, so that the line element becomes

$$ds^2 = -\alpha^2 dt^2 + a^2 dr^2 + r^2 d\Omega^2 \,. \tag{54}$$

As before, to construct star-like solutions, we adopt the time-harmonic ansatz (33) for the complex scalar field, adapt the time coordinate to the timelike Killing vector field, and require the spacetime to be static. We again find that the extrinsic curvature tensor vanishes identically (so that, for static data, the slicing is polar as well as maximal), and that the momentum constraint (13) is automatically satisfied.

Again, considering the Hamiltonian constraint, the Klein-Gordon equation, and the slicing condition

$$\dot{K^\theta}_\theta = 0 \,, \tag{55}$$

at $t = 0$, we have (dropping the subscript 0's as before):

$$a' = \frac{1}{2}\left\{\frac{a}{r}\left(1 - a^2\right)\right.$$
$$\left. + 4\pi r a\left[\phi^2 a^2\left(m^2 + \frac{\omega^2}{\alpha^2}\right) + \Phi^2\right]\right\} \,, \tag{56}$$

$$\alpha' = \frac{\alpha}{2}\left\{\frac{a^2 - 1}{r}\right.$$
$$\left. + 4\pi r\left[a^2\phi^2\left(\frac{\omega^2}{\alpha^2} - m^2\right) + \Phi^2\right]\right\} \,, \tag{57}$$

$$\phi' = \Phi \,, \tag{58}$$

$$\Phi' = -\left(1 + a^2 - 4\pi r^2 a^2 m^2 \phi^2\right)\frac{\Phi}{r}$$
$$- \left(\frac{\omega^2}{\alpha^2} - m^2\right)\phi a^2 \,. \tag{59}$$

In this case, the regularity conditions are

$$a(0) = 1 \,, \tag{60}$$
$$\Phi(0) = 0 \,, \tag{61}$$

while the outer boundary conditions are

$$\lim_{r \to \infty} \phi(r) \approx 0 \,, \tag{62}$$

$$\lim_{r \to \infty} \alpha(r) = \frac{1}{a(r)} \,. \tag{63}$$

As before, we can convert the last condition to an *inner* condition on α by taking advantage of the linearity and homogeneity of the slicing equation. Specifically, we can again choose $\alpha(0) = 1$, and then after integration of (56)–(59) simultaneously rescale $\alpha(r)$ as well as the eigenvalue, ω, so that (63) is satisfied.

We again consider the family of boson star solutions parametrized by the central value of the modulus of the scalar field, $\phi_0(0)$. In this case, given a value of $\phi_0(0)$, and using the conditions $a(0) = 1$, $\alpha(0) = 1$, $\Phi(0) = 0$, we need only adjust the eigenvalue ω itself in order to generate a solution with the appropriate asymptotic behaviour (i.e. so that $\lim_{r \to \infty} \phi(r) = 0$). This is a classic 1-parameter shooting problem, which is comparatively easier than the 2-parameter shooting method described above.

Once we have computed a solution in areal coordinates, we can perform a coordinate transformation from areal coordinates to isotropic coordinates [13, 14] (recall that the maximal and polar slices coincide for the static case). Essentially this amounts to solving an ODE of the form

$$r\,|_{R=R_{\max}} = \left[\left(\frac{1 + \sqrt{a}}{2}\right)^2 \frac{R}{a}\right]_{R=R_{\max}} \,,$$
$$\frac{dr}{dR} = a\frac{r}{R} \,. \tag{64}$$

We emphasize that (36)–(41) or (56)–(59) are used for generating initial data describing a spacetime that has no matter content other than a single boson star. To "perturb" a given boson star, and, in particular, to drive the star to the threshold of black hole formation, we implode a (spherical) shell of massless scalar field onto it. Specifically, we choose initial data for the massless field of the following "gaussian" form:

$$\phi_3(0, r) = A_3 \exp\left[-\left(\frac{r - r_0}{\sigma}\right)^2\right] \,, \tag{65}$$

where A_3, r_0 and σ are adjustable parameters, controlling the overall amplitude, position and width, respectively, of the imploding gaussian wave packet. To ensure that the massless field is almost purely in-going at the initial time, we specify the "conjugate" variable $\Pi_3 \equiv \psi^2/\alpha\left(\dot{\phi_3} - \beta\phi_3{}'\right)$ as follows:

$$\Pi_3(0, r) = -\left(\Phi_3(0, r) + \frac{\phi_3(0, r)}{r}\right) \,. \tag{66}$$

In all of our studies described below, we have fixed r_0 and σ in (65) to $r_0 = 40$ and $\sigma = 5$. This ensures that the support of the massless field is well separated from that of the complex field (i.e. from any of the boson stars *per se* that we study) at the initial time.

Once the complex scalar field, ϕ, and the real scalar field, ϕ_3, are known, the initial data for the functions $\psi(0, r)$, $K^r{}_r(0, r)$, $\alpha(0, r)$ and $\beta(0, r)$ are computed by solving the Hamiltonian constraint (12), the momentum constraint (13), the slicing condition (18), and the isotropic condition (19) respectively.

III. RESULTS

A. Setup of numerical experiments

The PDEs solved in the simulations discussed here are those listed in the previous section. We also provide a summary of the equations of motion of the system, the boundary conditions, and details of the finite difference approximation used in App. A. Additionally, results of convergence tests of our code are discussed in App. B.

In order to study critical behaviour in the model we start with initial data for the complex field that represents a boson star on the stable branch (i.e. a star with a central scalar field value $\phi_0(0) \lesssim 0.08$, using our units and conventions). We generally choose a configuration that is reasonably relativistic, i.e. with $\phi_0(0)$ bounded away from 0, but not too close to the instability point, $\phi(0) \approx 0.08$.

Details of the initial data setup were described in the previous section. Typical evolution of such initial data proceeds as follows. Once we have fixed the boson star configuration, we complete the specification of the massless scalar field initial data by fixing the overall amplitude factor, A_3, and then evolve the system. Initially, the shell of massless scalar field implodes towards $r = 0$ at the speed of light, while the boson star "sits" in its static state centered at the origin. As the in-going massless shell reaches the region of space occupied by the boson star, its contribution to the overall gravitational field tends to compress the boson star to a higher mean density and smaller radius. The massless field passes through the origin and then "explodes" outward, eventually propagating off the computational domain. Depending on the strength of the perturbation from the massless field, we find that the compressed boson star either relaxes to something resembling a stable boson star with large-amplitude oscillations, or collapses to form a black hole. Thus by adjusting the massless scalar amplitude factor, A_3—which we generically use as the adjustable parameter, p, in our study of critical behaviour in the model—we can tune the evolution to the threshold of black hole formation. In practice we use a bisection search to refine our estimate of the critical value, $A_3^\star$, and can carry the search to machine precision, so that $\Delta A_3 / A_3 \sim 10^{-15}$ using standard 8-byte floating-point arithmetic. Unless otherwise specified, the computations described below have been performed with a spatial mesh spacing $\Delta r = 50/1024 \approx 0.049$, a Courant factor $\Delta t / \Delta r = 0.3$, and the coefficient of Kreiss-Oliger dissipation, $\epsilon_d = 0.5$ (see App. A for the definition of ϵ_d).

We note that our numerical calculations generate entire *families* of critical solutions, fundamentally reflecting the fact that there is a continuum of one-mode unstable boson star configurations (see Fig. 3). In addition, for any fixed initial boson star state, the specifics of the observed threshold solution will depend on the details of the "perturbing" scalar field. This last fact is, however, irrelevant to the conclusions that we draw from our study.

In the following section we discuss results from detailed studies of black hole threshold solutions generated from several distinct initial boson star states. Table I summarizes the values of $\phi_0(0)$ that were used, the approximate values of A_3 required to generate a critical solution, the location, $r_{\max}$, of the outer boundary of the computational domain, and the figures that display results associated with the respective calculations. Since we will not dwell on this point below, we note that all of our calculations confirm the basic picture previously reported that the black holes that form just above threshold in this type of collapse generically have *finite* mass (i.e. that the critical transition is Type I).

B. Critical phenomena

We start by examining results from a critically perturbed boson star having an unperturbed central field value $\phi_0(0) = 0.05$. As just described, the critical massless amplitude factor, $A_3^\star \sim 0.0032$, was determined by performing a bisection search on A_3, to roughly machine precision. (Recall that each iteration in this search involves the solution of the time-dependent PDEs for the model for a specific value of A_3, with all other parameters held fixed, and the criterion by which we adjust the bisection bracket is whether or not the simulation results in black hole formation.)

A series of snapshots of $\partial M(t, r)/\partial r$ (where $M(t, r)$ is the mass aspect function) for a marginally subcritical evolution is shown in Fig. 1. Full analysis of the results of this simulation indicate that the boson star enters what we identify as the critical state at $t \approx 130$, and remains in that state until $t \approx 510$. It is worth noting that the boson star actually completes its collapse into a more compact configuration well after the real scalar field has dispersed from the boson star region. We also note that the amount of time, τ, spent in the critical state—$\tau \approx 380$ in this case—is a function of how closely the control parameter has been tuned to criticality. Specifically, we expect τ to be linear in $\ln |A_3 - A_3^\star|$ (see (1)), and we will display evidence for this type of scaling below.

Fig. 2 shows the time evolution of the central modulus of the complex scalar field for marginally subcritical evolutions generated from boson star initial states with $\phi_0(0) = 0.035, 0.04$ and 0.05. From the figure we can see that in all three cases the perturbed stars enter an excited, critical state at $t \approx 100$ and remain in that state for a finite time which is a function of $\phi_0(0)$ (i.e. of the initial state). Additionally, at least for the cases $\phi_0(0) = 0.035$, $\phi_0(0) = 0.04$, the figure provides evidence that following the critical evolution phase, the excited stars relax to states characterized by large amplitude oscillations of the complex field. This behaviour will be examined in more detail below. Finally, also apparent in the plot are the smaller-amplitude oscillations that occur during the periods of critical evolution. Previous work [1, 2] indicated

Fig.	ϕ_0	$A_3^{\star}$	$r_{\max}$
1	0.05	0.0032	50
2, 3	0.035, 0.04, 0.05	0.00471, 0.00342, 0.00316	50
4	0.02, 0.035, 0.04, 0.05	0.00915, 0.00471, 0.00342, 0.00316	50
5	0.04	0.00342	200
6	0.035, 0.04, 0.05	0.0083, 0.0061, 0.0031	100
7, 8	0.04	0.00342, 0.00603, 0.00623, 0.00632	50, 100, 200, 400

TABLE I: Summary of parameters used to generate the results displayed in Figs. 1-8. Listed for each distinct computation or numerical experiment are the relevant figure numbers, central amplitude of the complex field, $\phi_0(0)$, the overall massless scalar amplitude factor, $A_3^{\star}$ (see 65), that generates a marginally-critical solution, and the maximum radial coordinate, $r_{\max}$, of the computational domain. Other parameters defining the massless scalar initial profile (65) are held fixed at $r_0 = 40$, $\sigma = 5$ for all simulations. Other numerical parameters are chosen to be $\Delta r = 50/1024 \approx 0.049$, $\Delta t / \Delta r = 0.3$ and $\epsilon_d = 0.5$, and are also fixed for the calculations discussed here.

that these oscillations can be interpreted as excitations of the (stable) first *harmonic* mode of the unstable boson star that is acting as the critical solution—the unstable *fundamental* mode is the one that determines whether or not the configuration will evolve to a black hole. Although we have not studied this matter in any detail, we assume that the same picture holds for our current calculations.

The results from our simulations of critically perturbed boson stars are thus in agreement with the previous studies [1, 2] which identified the critical states as excited (primarily in the first harmonic mode), unstable boson stars. Following that work we display in Fig. 3 an approximate correspondence between the initial boson stars and the critical solutions. The solid line traces the one-parameter family of static boson stars (parameterized as usual by $\phi_0(0)$), where we have defined the radius, R, of a boson star so that $M(R) = 0.99\, M(\infty) = 0.99\, M_{\mathrm{ADM}}$. The triangles indicate the initial stable boson star configurations, the squares indicate our best estimate of the corresponding unstable critical boson star states, and each arrow schematically depicts the transition between the two states that is induced by the perturbing scalar field. We note that to identify which unstable boson star is acting as the critical solution—which is equivalent to identifying an effective value of $\phi_0(0)$—we time average the central modulus of the complex field, $|\phi(t,0)|$ during the period of critical evolution. In addition, in accord with previous results, we observe that in all cases the mass of the unstable critical state is *larger* than that of the progenitor boson star, indicating that a significant amount of mass-energy is extracted from the massless scalar field through its purely gravitational interaction with the complex field.

As discussed previously, for both subcritical and supercritical simulations, the closer one tunes A_3 to the critical value $A_3^{\star}$, the longer the perturbed star will persist in the critical state. Specifically, we observe scaling of the lifetime, τ, of the critical evolution of the form

$$\tau(A_3) \sim -\gamma \ln |A_3 - A_3^{\star}|, \qquad (67)$$

where we define the lifetime to be the lapse of coordinate time from the start of the evolution, $t = 0$, to the time of first detection of an apparent horizon, and where γ is a scaling exponent that depends on which of the infinitely many one-mode unstable boson stars acts as the critical solution in the particular scenario being simulated. We note that the details of the definition of τ are not important to the determination of γ in (67) since γ actually measures the *differential* in lifetime with respect to changes in $A_3 - A_3^{\star}$, and this differential is insensitive to precisely how we define τ, at least as $A_3 \to A_3^{\star}$. In addition, we note that in using coordinate time in our definition of the scaling relationship (67), we are defining the scaling with respect to proper time at spatial infinity. Another choice—arguably more natural—would be to define τ in terms of the proper time measured by an observer at rest at $r = 0$ (central proper time). Since the critical solutions are nearly static, the relation between these two different definitions of time would be a specific factor for each distinct value of $\phi_0(0)$, and would thus lead to a $\phi_0(0)$-dependent "renormalization" of the scaling exponents, γ.

Fig. 4 shows measured scaling laws from supercritical evolutions of perturbed boson stars defined by $\phi_0(0) = 0.02, 0.035, 0.04$ and 0.05. It is clear from these plots that, at least as $A_3 \to A_3^{\star}$, we have lifetime scaling of the form (67). Estimated values of γ—computed from linear least-squares fits to the plotted data—are $\gamma = 8.1, 11, 14, 17$ for $\phi_0(0) = 0.02, 0.035, 0.04, 0.05$, respectively. We note that according to the now standard picture of critical collapse (see for example [4]), each value of γ can be identified with the reciprocal Lyapunov exponent (i.e. growth factors) of the single unstable mode associated with the corresponding critical solution. Again, the reason that we observe different values of γ for different choices of initial boson star (different values of $\phi_0(0)$) is that distinct critical solutions are being generated in the various cases. That is, we cannot expect universality (with respect to initial data) in this case because the model admits an entire family of one-mode unstable solutions that sit at the threshold of black
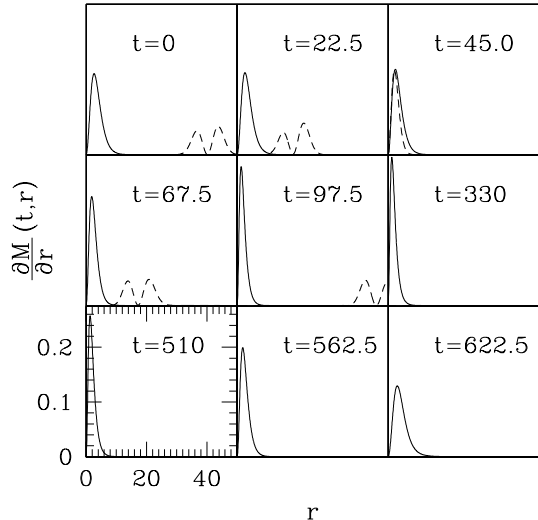
FIG. 1: Critical evolution of a perturbed boson star with $\phi_0(0) = 0.05$ and mass, $M_{\rm ADM} = 0.62$ (using our units and conventions). This figure shows the time development of contributions to $\partial M/\partial r$ from the complex (solid line) and real (dashed line) scalar fields. Note that the temporal spacing between successive snapshots is *not* constant—the time instants displayed have been chosen to illustrate the key features of the near-critical evolution. Also note that we have multiplied the value of $\partial M/\partial r$ for the *real* scalar field by a factor of 8 to aid in the visualization of that field's dynamics. The evolution begins with a stable boson star centered at the origin, and an in-going gaussian pulse (shell) of massless, real scalar field that is used to perturb the star. The overall amplitude factor, A_3, of the initial real scalar field profile (see (65)), is the control parameter for generating the one-parameter family of solutions that interpolates through the black hole threshold. For the calculation shown here, A_3 has been tuned to a critical value $A_3^\star \approx 0.0032$ via a bisection search (and with a fractional precision of $\approx 10^{-15}$). The other parameters defining the gaussian initial profile of the massless field are $r_0 = 40$ and $\sigma = 5$. The snapshots show that the real scalar field enters the region containing the bulk of boson star at $t \approx 22$, implodes through the origin at $t \approx 45$, leaves the boson star region at $t \approx 70$, and, finally, completely disperses from the computational domain at $t \approx 100$. The boson star enters the critical state at roughly the same time that the real field leaves the domain, and remains in that state for a period of time which is long compared to the crossing time of the massless field. At $t \approx 510$, the boson star begins to depart significantly from the critical state.

hole formation.

C. Final Fate of Subcritical Evolutions

In previous work on the problem of critically perturbed spherically symmetric boson stars [1, 2], it was conjec-
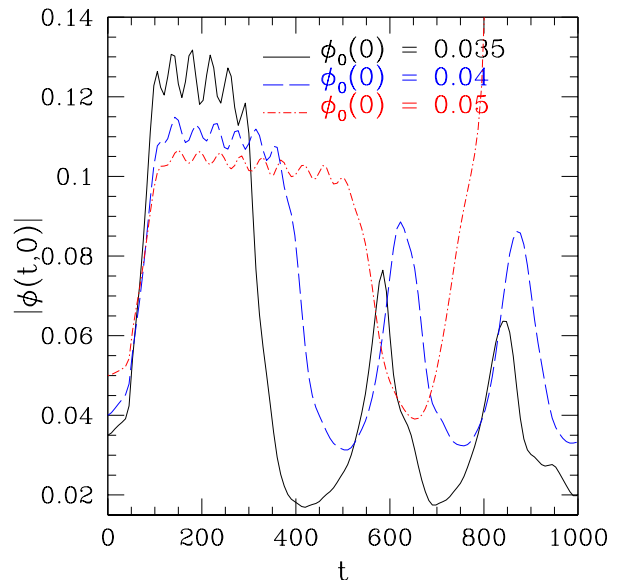

FIG. 2: Time evolution of the central value of the scalar field modulus for subcritical evolution of perturbed boson stars. The figure shows the time evolution of $|\phi(t,0)|$ for marginally subcritical evolutions generated from boson star initial states with $\phi_0(0) = 0.035, 0.04$ and 0.05. See the text for a description of key features of this plot.

tured that the end state of subcritical evolution was characterized by *dispersal* of the boson star to large distances (relative to the size of the initial, stable star). This conjecture was at least partially influenced by the behaviour observed, for example, in the collapse of a *massless* scalar field [3], where subcritical evolutions *do* involve complete dispersal of the field. However, another key reason for what we claim is a misidentification of the true subcritical end-state, was that the simulations described in [1, 2] simply were not carried out for sufficient coordinate time to observe the nature of the late-time dynamics. Our current simulations strongly suggest that subcritical evolutions lead to a "relaxation" of the critically perturbed state to something that approximates a boson star (not necessarily the original star) undergoing large amplitude oscillations. As argued in the next subsection, these oscillations can largely be identified with the fundamental perturbative mode associated with the final boson star state. The numerical evidence also suggests that, at least in many cases, these oscillating configurations eventually *re-collapse* and form black holes; a "prompt" re-collapse can be seen in the $\phi_0(0) = 0.05$ data in Fig. 2.

Fig. 5 displays the long-time behaviour of $\max_r(2M(t,r)/r)$, $|\phi(t,0)|$ and $\psi(t,0)$ for a near-critically perturbed boson star ($\phi_0(0) = 0.04, A_3^\star \approx 0.00342$) for $r_{\max} = 200$ (with mesh spacing $\Delta r = 200/4096 \approx 0.049$). Note that this is a *subcritical* evolution, so that a black hole does *not* form. As shown in more detail in previous figures, the boson
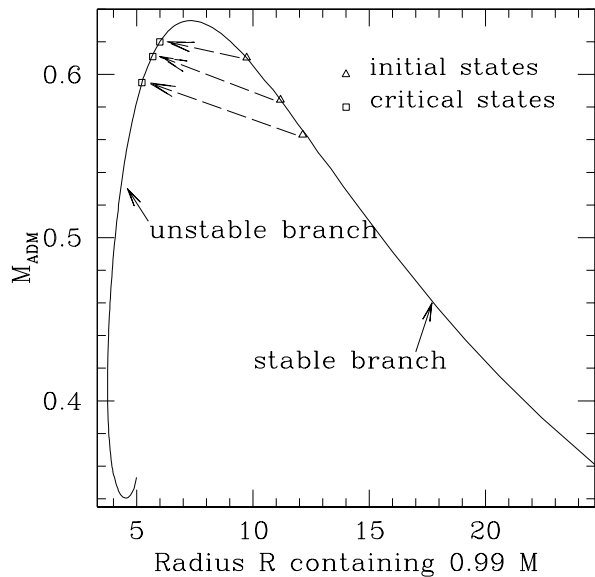
FIG. 3: Transition of perturbed boson stars in critical evolutions. The solid curve shows the parametric mass *vs* radius plot of static boson stars (curve parameter $\phi_0(0)$ increasing from right to left), where we have defined the stellar radius, R, so that $M(R) = 0.99\,M(\infty) = 0.99\,M_{\rm ADM}$. Triangles label the initial configurations, squares show the corresponding critical solutions (identified as one-mode-unstable boson stars with oscillations that are largely in the fundamental mode), and the dashed arrows represent schematically the transition between the initial and critical states. See the text for more details.
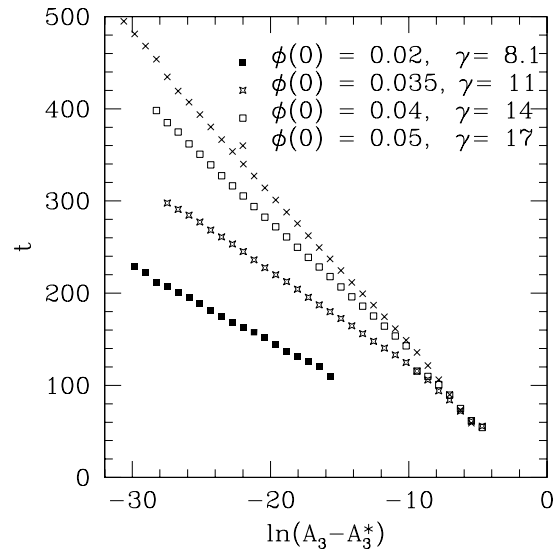

FIG. 4: Measured lifetime scaling laws for critically perturbed boson stars. This figure shows the measured lifetimes of various near-critical evolutions of perturbed boson stars as a function of $\ln|A_3 - A_3^\star|$, for cases with $\phi(0) = 0.02, 0.035, 0.04$ and 0.05. Quoted scaling exponents, γ (see (67)), are computed from linear least-squares fits to the data. The apparent convergence of the data for different $\phi_0(0)$ as $\ln|A_3 - A_3^\star| \to 0$ is not significant, as it reflects calculations *far* from criticality i.e. far from the $\ln|A_3 - A_3^\star| \to -\infty$ limit. See the text for additional details.

star enters a critical state (well approximated by an unstable boson star) shortly after the real scalar field leaves the computational domain ($t \approx 100$). While in the critical state, the star oscillates with what we assume is the frequency of the first harmonic, as computed from perturbation theory using the unstable boson star state as the background (see [1, 2]). At $t \approx 300$ the star begins to evolve away from the more compact critical configuration, decreases in central density, expands in size, and starts to pulsate with a different frequency. Although at late time the oscillation amplitudes are much larger than those seen in the critical phase of evolution, we will show in the following section that the oscillations can nonetheless be largely attributed to excitations of the fundamental perturbative mode associated with the final boson star state.

Fig. 6 shows the long-time behaviour of the modulus of the central value of scalar field, $|\phi(t,0)|$, for initial configurations with $\phi_0(0) = 0.035, 0.04$ and 0.05, with $r_{\rm max} = 100$, but with Δr maintained at $50/1024$ as in Fig. 5. Again, we use A_3 to tune the evolution of the boson stars to criticality and the figure shows a marginally subcritical evolution. In general, the computed value of $A_3^\star$ is a function of $r_{\rm max}$, as is the specific stable boson star to which the critical evolution relaxes. However, the

results shown in the figure support our claim that an oscillatory phase (rather than dispersal) *generically* follows near-critical evolution of driven boson stars in the marginally subcritical case.

Fig. 7 shows the long time behaviour of subcritical evolution of the modulus of the central scalar field value, $|\phi(t,0)|$, with an initial boson star given by $\phi_0(0) = 0.04$. Here, we vary the position of the outer edge of the computational domain $r_{\rm max}$, while keeping the resolution, Δr, fixed at $50/1024$ as previously. For each of $r_{\rm max} = 50, 100, 200$ and 400, we tune A_3 to generate a critical evolution (the specific values of $A_3^\star$ obtained are listed in Table I). This set of calculations provides evidence for the convergence of the critical solution (including the critical value of the control parameter, A_3), as $r_{\rm max} \to \infty$ at fixed resolution. This in turn strongly suggests that the final oscillatory states identified in subcritical evolutions are not artifacts of our use of a finite computational domain.

In order to illuminate the nature of typical post-critical oscillations, Fig. 8 shows the square of the discrete fast Fourier transform, $\mathcal{F}\left[|\phi(t,0)|\right]$, of the central scalar field modulus for the same set of simulations used to prepare Fig. 7. The transform is taken for discrete times, t^n, satisfying $2500 \lesssim t^n \lesssim 7000$, a period when the boson
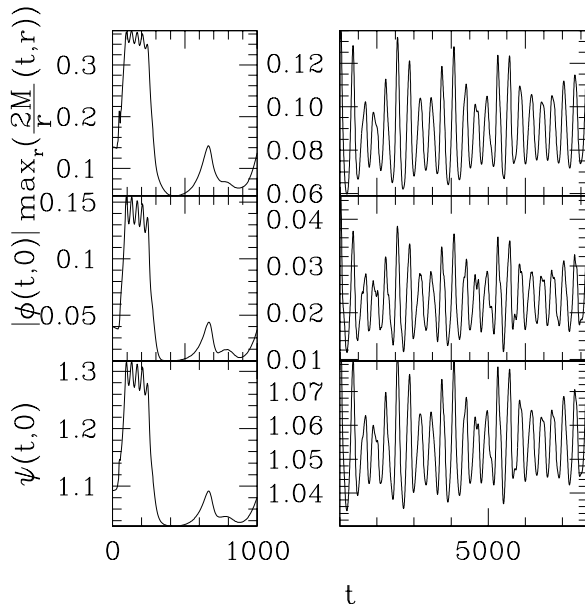
FIG. 5: Long time behaviour of subcritical evolution for $\phi(0,0) = 0.04$ with $r_{\max} = 200$. This figure shows the long-time behaviour of $\max_r(2M(t,r)/r)$, $|\phi(t,0)|$ and $\psi(t,0)$ for a near-critically perturbed boson star ($\phi_0(0) = 0.04$, $A_3^\star \approx 0.00342$). The left side of the figure shows the evolution of the perturbed star in its critical state ($100 \lesssim t \lesssim 300$), and the evolution shortly after the star leaves its critical state. The right side of the figure focuses on oscillations seen at later times $1000 \leq t \leq 7680$. These plots provides evidence that the final state of subcritical evolution is characterized by large amplitude oscillations about something approximating a boson star on the stable branch, rather than dispersal of the complex field as suggested in [1, 2]. Detailed calculation (see Sec. III D) shows that the pulsation frequency is approximately the fundamental mode frequency computed from perturbation theory about a background stable boson star solution with $\phi_0(0) = 0.023$. We also note the overall lower-frequency modulation of the post-critical oscillations. This effect is not yet understood, although one possible explanation—namely that the envelope modulation represents "beating" of the fundamental and first harmonic modes—appears to be ruled out.

star has undergone the transition from critical evolution to post-critical oscillation. The figure clearly shows the convergence of the fundamental mode oscillation, as well as a first harmonic. The next section provides a more detailed analysis of the observed fundamental mode excitations.

D. Perturbation Analysis of Subcritical Oscillations

We now proceed to an application of perturbation theory to the oscillations seen in long-time evolutions
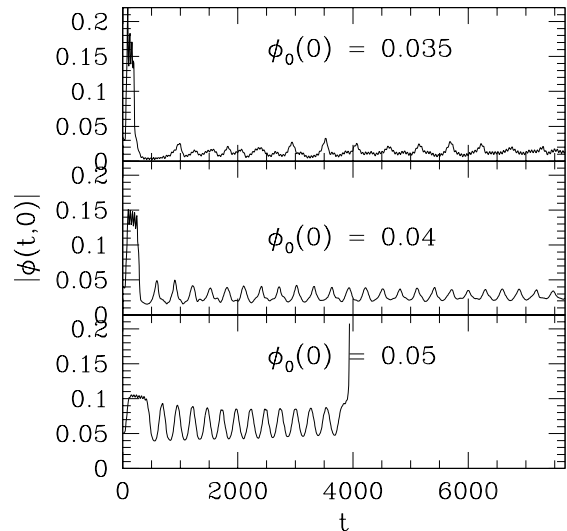

FIG. 6: Long time behaviour of subcritical evolution with initial configurations $\phi_0(0) = 0.035, 0.04$ and 0.05, for $r_{\max} = 100$. The figures show the modulus of the central scalar field values, $|\phi(t,0)|$, vs time, using the same resolution $\Delta r = 50/1024$ used to generate the data shown in Fig. 5. Each of the three distinct boson stars is driven to a different critical solution, and subsequently relaxes to a different final oscillatory state. This provides evidence that the final end state of marginally subcritical evolution in generic driven boson stars does *not* involve dispersal of the bulk of the complex field to infinity.

of marginally subcritical configurations, such as those shown in Fig. 5. Here we follow [15] and [2], and refer the interested readers to those sources for details of the approach that we do no include here. In particular, we emphasize that we have *not* carried out the complete perturbation analysis ourselves, but are simply using a computer code provided by Hawley [5] to analyze our current simulations. Nonetheless, to make contact between the perturbative and simulation results, it is useful to briefly review the setup of the perturbative problem.

To formulate the equations for the perturbation analysis, we first rewrite the complex scalar field as

$$\phi(t,r) = (\psi_1(t,r) + i\psi_2(t,r))\, e^{-i\omega t}, \qquad (68)$$

(Note that this representation is distinct from $\phi = \phi_1 + i\phi_2$, and the reader should be careful not to confuse the ψ's used here with the conformal metric variable, ψ.) Additionally, the spacetime metric is written in Schwarzschild-like (polar-areal) coordinates:

$$ds^2 = -e^{\nu(t,r)}dt^2 + e^{\lambda(t,r)}dr^2 + r^2\left(d\theta^2 + \sin^2\theta d\varphi^2\right). \quad (69)$$
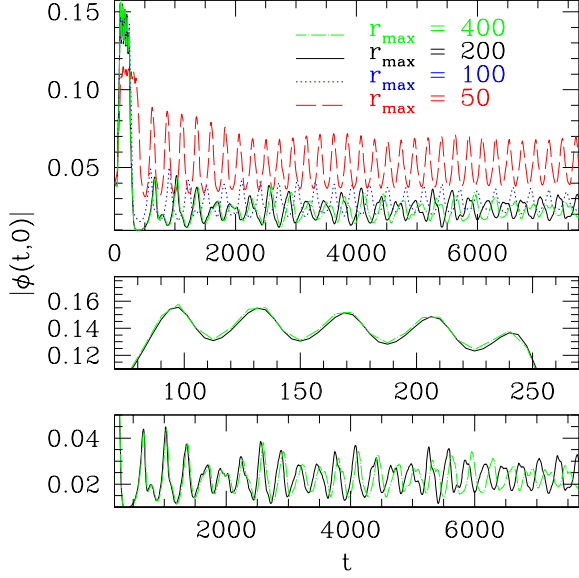
We further introduce four perturbation fields,

FIG. 7: Long time behaviour of subcritical evolution with an initial boson star characterized by $\phi_0(0) = 0.04$, for $r_{\max} = 50, 100, 200$ and 400. The figures show the modulus of the central scalar field values, $|\phi(t,0)|$, *vs* time, with the resolution Δr fixed at $50/1024$ as in previous figures. The evolutions are tuned to criticality for different $r_{\max}$ (see Table I). The top figure shows the overall evolutions for $r_{\max} = 50, 100, 200$ and 400 from $t = 0$ to $t = 7680$. The middle figure focuses on the evolution of the perturbed boson star during the period of near-critical evolution, $70 \leq t \leq 270$, for the cases $r_{\max} = 200$ and 400. The near coincidence of the two curves in this case provides strong evidence for convergence of our calculations (at fixed spatial resolution) as $r_{\max} \to \infty$. The bottom figure focuses on the late time evolution—$200 \leq t \leq 7680$—again for $r_{\max} = 200$ and 400, and provides additional support for our claim that the final oscillatory states we observe in subcritical evolution are not an artifact of the use of a finite computational domain.

FIG. 8: Long time behaviour of subcritical evolution with an initial boson star characterized by $\phi_0(0) = 0.04$, for $r_{\max} = 50, 100, 200$ and 400. The figures show the square of the (discrete) Fourier transform $\mathcal{F}[|\phi(t,0)|]$, of the central scalar field modulus, using the same calculations described in Fig. 7. The transform is taken from a data set defined at 691 discrete times, t^n satisfying $2500 \lesssim t^n \lesssim 7700$, during which time the critically perturbed boson star is in its final oscillatory state. Again, the resolution, $\Delta r = 50/1024$, is the same used in previous calculations The fundamental mode computed for the case $r_{\max} = 200$ is approximately $\omega \approx 33 \times 6 \times 10^{-4} = 0.0198$, in good agreement with our perturbation-theory estimate computed in Sec. III D. The figure shows that the computed frequency of the fundamental mode converges for increasing $r_{\max}$. The graph also shows evidence for at least one higher overtone which persists as $r_{\max} \to \infty$. The figure inset shows the overall amplitudes of the computed Fourier components.

$\delta\lambda(t,r), \delta\nu(t,r), \delta\psi_1(t,r)$ and $\delta\psi_2(t,r)$, which represent the perturbations about the equilibrium values $\lambda_0(r), \nu_0(r), \phi_0(r)$:

$$\lambda(t,r) = \lambda_0(r) + \delta\lambda(t,r), \tag{70}$$

$$\nu(t,r) = \nu_0(r) + \delta\nu(t,r), \tag{71}$$

$$\psi_1(t,r) = \phi_0(r)\left(1 + \delta\psi_1(t,r)\right), \tag{72}$$

$$\psi_2(t,r) = \phi_0(r)\delta\psi_2(t,r). \tag{73}$$

With the above definitions we can write the coupled Einstein-Klein-Gordon field equations as a set of PDEs for the functions $\delta\lambda, \delta\nu, \delta\psi_1$ and $\delta\psi_2$. With some manipulation we can then eliminate $\delta\nu$ and $\delta\psi_2$ to produce a system of two coupled second-order PDEs for $\delta\psi_1$ and $\delta\lambda$:
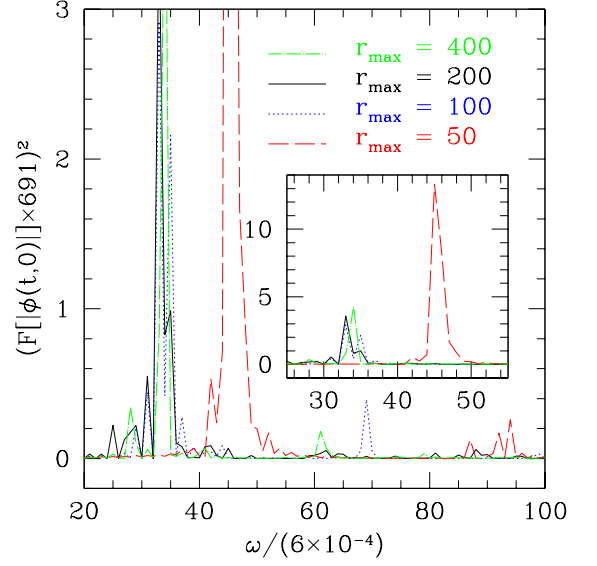
$$\begin{aligned}
\delta\psi_1'' &= -\left(\frac{2}{r} + \frac{\nu_0' - \lambda_0'}{2}\right)\delta\psi_1' - \frac{\delta\lambda'}{r\phi_0{}^2} + e^{\lambda_0 - \nu_0}\ddot{\delta\psi_1} \\
&\quad - \left[\frac{\phi_0'}{\phi_0}\left(\frac{\nu_0' - \lambda_0'}{2} + \frac{1}{r}\right) + \left(\frac{\phi_0'}{\phi_0}\right)^2\right. \\
&\qquad\left. + \frac{1 - r\lambda_0'}{r^2\phi_0{}^2} + e^{\lambda_0 - \nu_0}\omega^2 - e^{\lambda_0}\right]\delta\lambda \\
&\quad + 2e^{\lambda_0}\left[1 + e^{-\nu_0}\omega^2\right. \\
&\qquad\left. + e^{-\lambda_0}\left(\frac{\phi_0'}{\phi_0}\right)^2 + r\phi_0\phi_0'\right]\delta\psi_1, \tag{74}
\end{aligned}$$

$$\delta\lambda'' = -\frac{3}{2}\left(\nu_0' - \lambda_0'\right)\delta\lambda' + \left[4\phi_0'^2 + \lambda_0''\right.$$

$$+ \frac{2}{r^2} - \frac{(\nu_0' - \lambda_0')^2}{2} - \frac{2\nu_0' + \lambda_0'}{r}\left]\delta\lambda\right.$$

$$+ e^{\nu_0 - \nu_0}\ddot{\delta\lambda} - 4\left(2\phi_0\phi_0' - re^{\lambda_0}\phi_0^2\right)\delta\psi_1'$$

$$- 4\left[2\phi_0'^2 - re^{\lambda_0}\phi_0^2\right.$$

$$\left.\times\left(2\frac{\phi_0'}{\phi_0} + \frac{2\nu_0' + \lambda_0'}{2}\right)\right]\delta\psi_1. \qquad (75)$$

Note that these equations involve only second time derivatives (i.e. there are no terms involving $\dot{\delta\psi}_1$ or $\dot{\delta\lambda}$), and that they are *linear* in the second time derivatives. If we thus assume a harmonic time-dependence for the perturbed fields:

$$\delta\psi_1(t,r) = \delta\psi_1(r)e^{i\sigma t}, \qquad (76)$$

$$\delta\lambda_1(t,r) = \delta\lambda_1(r)e^{i\sigma t}, \qquad (77)$$

then the equations for the perturbations contain σ only in the form σ^2, and the sign of σ^2, as computed by solving a particular mode equation, determines the stability of that mode. (Note that the system can be shown to be self-adjoint so that the values of σ^2 must be real.) If any of the values of σ^2 are found to be negative, then the associated perturbations will grow and the boson star will be unstable. Moreover, as the eigenvalues form an infinite discrete ordered sequence, examining the fundamental radial mode σ_0^2 determines the overall stability of any particular star with respect to radial perturbations.

In order to compare the simulation results with those given by perturbation theory, we first observe that there is a difference in the choice of the time coordinates used in the two calculations. Specifically, in the perturbative analysis [2, 15], the lapse is chosen to be unity at the origin, so we have

$$\sigma^2\Big|_{\text{perturbative}} \rightarrow \frac{\sigma^2}{\alpha^2}\Big|_{\text{simulation}}.$$

We also note that there is a factor of 2 difference in the definitions of $T_{\mu\nu}$ used in the two calculations, and that the definition of the complex field, $\phi(t,r)$, in the perturbative calculation includes a factor of $\sqrt{8\pi}$. We thus have

$$\phi\Big|_{\text{perturbative}} \rightarrow \sqrt{4\pi}\phi\Big|_{\text{simulation}}.$$

The numerical technique for obtaining the fundamental mode and first harmonic mode frequencies of boson stars has already been described in [2] and will not be repeated here; again, we will simply quote and use results from that study. From Fig. 5 we note that there

are 10 oscillations between $t = 2553.8$ and $t = 5583.8$, giving a period $T \approx 333$. Hence we have an oscillation frequency $\sigma = 2\pi/T \approx 0.019$. The time average of the lapse function, $\langle\alpha(t,0)\rangle_t$, in the interval is 0.89, and so $\sigma^2/\alpha^2 \approx 0.00045$. We also compute the time average of $\phi(t,0)$ in the interval, and use the resulting value to identify the stable boson star solution about which we perform the perturbation analysis. We find $\langle\phi_0(t,0)\rangle_t \approx 0.023 \times \sqrt{4\pi} = 0.0815$. For a boson star with $\phi_0(0) = 0.0815$, the perturbative calculations (see Fig. 7 of [2]) predict $\sigma_0^2 = 0.00047$, which is in reasonable agreement with the simulation results. Hence the oscillations that occur in the post-critical regime appear to be largely fundamental mode oscillations of a final-state, stable, boson star. We also remark that since the oscillations are of such large amplitude, it does not appear possible to precisely identify an effective background state (i.e. an effective value of $\phi_0(0)$), so the level of agreement in the oscillation frequencies is probably as good as one could expect.

IV. SUMMARY

We have investigated type I critical phenomena of ground state boson stars in maximal-isotropic coordinates by perturbing the stars with in-going pulses of a real scalar field. In particular, contrary to previous claims, we find that the end state of generic subcritical evolution is a stable boson star executing large amplitude oscillations, and that the oscillations can be largely understood as excitations of the fundamental normal mode of the end-state star. For the particular example that we examined in detail, the oscillation frequency of the post-critical state was estimated to be $\sigma^2/\alpha^2 \approx 0.00045$, in good agreement with the frequency of the fundamental mode computed in perturbation theory, $\sigma_0^2 = 0.00047$.

APPENDIX A: FINITE DIFFERENCE ALGORITHM

Here we present the details of the numerical method used in our computations. We solve the PDEs (12)–(19) by a finite difference method. We replace the (t,r) continuum by a discrete lattice of grid points, and approximate the continuum field quantities $\mathcal{F} = \{\alpha, \beta, \psi, K^r{}_r, \phi_i, \Phi_i, \Pi_i\}$, where $i = 1, 2, 3$, by a set of

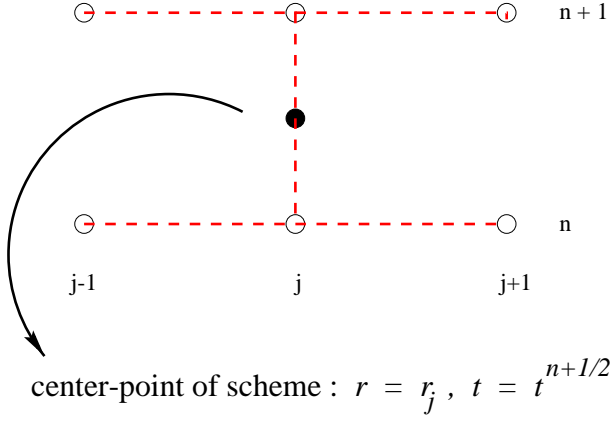center-point of scheme : $r = r_j$, $t = t^{n+1/2}$

FIG. 9: Stencil for an $O(h^2)$ Crank-Nicholson scheme for a PDE in one space dimension and time.

grid functions $\mathcal{F}^h = \{\alpha^h, \beta^h, \psi^h, K^r{}_r{}^h, \phi_i^h, \Phi_i^h, \Pi_i^h\}$ which are solutions of the finite difference approximation (FDA) of the PDEs. Denoting the uniform (constant) spatial and temporal mesh spacings by Δr and Δt, respectively, the finite difference grid is given by (t^n, r_j) where $r_j = r_0 + (j-1)\Delta r$, $j = 1, \cdots, N_r$ and $t^n = n\Delta t$, $n = 0, \cdots, N_t$. For any grid function $u^h \in \mathcal{F}^\langle$, the value at (t^n, r_j) is denoted by u_j^n and is an approximation of the continuum value $u(t^n, r_j)$.

In discretizing evolution equations (14)−(16) we make exclusive use of Crank-Nicholson schemes, with second order spatial differences. The key idea of a Crank-Nicholson method is to keep the differencing *centred* in time as well as in space, and a typical stencil used for such a scheme is illustrated in Fig. 9. The constraint equations (12) and (13) are coupled, nonlinear, ordinary differential equations, and following $O(\Delta r^2)$ finite differencing (see below) and are solved using a point-wise Newton's method. That is, at each grid point, (t^n, r_j), we solve for the pair $(\psi_j^n, (K^r{}_r)_j^n)$ using Newton's method for two equations in two unknowns. The slicing condition (18) is linear, so, after being discretized using second-order finite differences, can be solved directly using a tridiagonal solver. Finally, once the values α_j^n and $K^r{}_{rj}{}^n$ have been computed, an $O(\Delta r^2)$ discretization of (19) is easily integrated to yield the β_j^n.

To aid in the presentation of the finite difference equations, it is convenient to define the following difference operators:

$$\Delta^t_+ u_j^n = \frac{u_j^{n+1} - u_j^n}{\Delta t},$$

$$\Delta^r_0 u_j^n = \frac{u_{j+1}^n - u_{j-1}^n}{2\Delta r},$$

$$\Delta^r_{0b} u_j^n = \frac{3u_j^n - 4u_{j-1}^n + u_{j-2}^n}{2\Delta r},$$

$$\Delta^r_\pm u_j^n = \frac{\pm u_{j\pm 1}^n \mp u_j^n}{\Delta r},$$

$$\Delta^{\frac{r}{2}}_0 u_j^n = \frac{u_{j+\frac{1}{2}}^n - u_{j-\frac{1}{2}}^n}{\Delta r},$$

$$\Delta^{r^2}_0 u_j^n = \frac{u_{j+1}^n - u_{j-1}^n}{r_{j+1}{}^2 - r_{j-1}{}^2},$$

$$\Delta^{r^3}_0 u_j^n = \frac{u_{j+1}^n - u_{j-1}^n}{r_{j+1}{}^3 - r_{j-1}{}^3}.$$

$$\Delta^{\frac{r^3}{2}}_0 u_j^n = \frac{u_{j+\frac{1}{2}}^n - u_{j-\frac{1}{2}}^n}{r_{j+\frac{1}{2}}{}^3 - r_{j-\frac{1}{2}}{}^3},$$

and the averaging operator

$$\mu^t_\pm u_j^n = \frac{1}{2}\left(u_j^{n\pm 1} + u_j^n\right),$$

$$\mu^r_\pm u_j^n = \frac{1}{2}\left(u_{j\pm 1}^n + u_j^n\right).$$

We also define $\bar{\mu}^r_\pm$, which has the same definition as $\mu^r_\pm$, but which has a higher precedence over other algebraic operations, e.g.,

$$\bar{\mu}^r_+ \left(\frac{fg^2}{h}\right)_j^n = \frac{(\bar{\mu}^r_+ f_j^n)(\bar{\mu}^r_+ g_j^n)^2}{\bar{\mu}^r_+ h_j^n}.$$

The FDAs of the Klein-Gordon equations can then be written as:

$$\Delta^t_+ (\phi_i)_j^n = \mu^t_+ \left(\frac{\alpha}{\psi^2}\Pi_i + \beta\Phi_i\right)_j^n, \qquad (A1)$$

$$\Delta^t_+ (\Phi_i)_j^n = \mu^t_+ \Delta^r_0 \left(\beta\Phi_i + \frac{\alpha}{\psi^2}\Pi_i\right)_j^n, \qquad (A2)$$

$$\Delta_+^t (\Pi_i)_j^n = \mu_+^t \left\{ \frac{3}{(\psi^4)_j^n} \Delta_0^{r^3} \left[r^2 \psi^4 \left(\beta \Pi_i + \frac{\alpha}{\psi^2} \Phi_i \right) \right]_j^n \right.$$
$$- \left[\alpha \psi^2 m^2 \phi_i (1 - \delta_{i3}) \right]_j^n$$
$$\left. - \left[(\alpha K^r{}_r)_j^n + 2\beta_j^n \frac{\Delta_0^r (r\psi^2)_j^n}{(r\psi^2)_j^n} \right] (\Pi_i)_j^n \right\} \quad (A3)$$

where $i = 1, 2, 3$.

The FDA of the Hamiltonian constraint is

$$\frac{3}{(\psi_j^n)^5} \Delta_0^{\frac{r^3}{2}} \left(r_j^2 \Delta_0^{\frac{r}{2}} \psi_j^n \right) + \frac{3}{16} (K^r{}_r)_j^{n\,2}$$
$$= -\pi \left(\frac{\sum_{i=1}^3 \left(\Phi_i^2 + \Pi_i^2 \right)}{\psi^4} + m^2 \sum_{i=1}^2 \phi_i^2 \right)_j^n \quad (A4)$$

and the FDA of the momentum constraint is

$$\bar{\mu}_-^r (\psi_j^n)^2 \ \Delta_-^r (K^r{}_r)_j^n + 3 \Delta_-^r (r\psi^2)_j^n \bar{\mu}_-^r \left(\frac{K^r{}_r}{r} \right)_j^n$$
$$= \bar{\mu}_-^r \left[-8\pi \sum_{i=1}^3 \Pi_i \Phi_i \right]_j^n . \quad (A5)$$

Similarly, the FDAs for the maximal-isotropic conditions are

$$\Delta_+^r \Delta_-^r \alpha_j^n \ + \ \frac{2}{(r\psi^2)_j^n} \Delta_0^{r^2} \left(r^2 \psi^2 \right)_j^n \Delta_0^r \alpha_j^n$$
$$+ \left[4\pi m^2 \psi^4 \sum_{i=1}^2 \phi_i^2 \right.$$
$$\left. - 8\pi \sum_{i=1}^3 \Pi_i^2 - \frac{3}{2} (\psi^2 K^r{}_r)^2 \right]_j^n \alpha_j^n$$
$$= 0, \quad (A6)$$

and

$$r_{j-\frac{1}{2}} \Delta_-^r \left(\frac{\beta}{r} \right)_j^n = \mu_-^r \left[\frac{3}{2} \alpha K^r{}_r \right]_j^n, \quad (A7)$$

respectively, where $r_{j-\frac{1}{2}} \equiv (r_j + r_{j-1})/2$.

The regularity conditions are implemented as

$$\psi_1^n = \frac{4\psi_2^n - \psi_3^n}{3}, \quad (A8)$$
$$(K^r{}_r)_1^n = 0, \quad (A9)$$
$$\alpha_1^n = \frac{4\alpha_2^n - \alpha_3^n}{3}, \quad (A10)$$

$$\mu_+^t \left((\phi_i)_1^n - \frac{4(\phi_i)_2^n - (\phi_i)_3^n}{3} \right) = 0, \quad (A11)$$
$$(\Phi_i)_1^n = 0, \quad (A12)$$
$$\mu_+^t \left((\Pi_i)_1^n - \frac{4(\Pi_i)_2^n - (\Pi_i)_3^n}{3} \right) = 0, \quad (A13)$$

for all i and n. The outer boundary conditions are

$$\Delta_+^t \Phi_{i\,j}^n + \mu_+^t \left(\Delta_{0b}^r \Phi_{i\,j}^n + \frac{\Phi_{i\,j}^n}{r_j} \right) = 0, \quad (A14)$$
$$\Delta_+^t \Pi_{i\,j}^n + \mu_+^t \left(\Delta_{0b}^r \Pi_{i\,j}^n + \frac{\Pi_{i\,j}^n}{r_j} \right) = 0. \quad (A15)$$

We also adopt a scheme for numerical dissipation given by Kreiss and Oliger [16]. In other words an additional term

$$\mu_+^t \left(\Delta_{+KO}^t \Phi_{i\,j}^n \right)$$

is added to the right hand side of (A2), for $3 \le j \le N_r - 2$ (and similarly to the right hand side of (A3) for the Π_i), where Δ_{+KO}^t is defined by

$$\Delta_{+KO}^t u_j^n = -\frac{\epsilon_d}{16\Delta t} \left(u_{j+2}^n - 4u_{j+1}^n \right.$$
$$\left. + 6u_j^n - 4u_{j-1}^n + u_{j-2}^n \right). \quad (A16)$$

Here, ϵ_d is an adjustable parameter satisfying $0 \le \epsilon_d < 1$, and is typically chosen to be 0.5. We note that the addition of Kreiss-Oliger dissipation changes the truncation error of the FDAs at $O(\Delta t^3, \Delta r^3)$ and thus does *not* effect the leading order error of a second order ($O(\Delta t^2, \Delta r^2)$) scheme. The dissipation is useful for damping high frequency solution components that are often associated with numerical instability.

APPENDIX B: CONVERGENCE TESTING

Here we present the results of a convergence test of the code that evolves boson stars in spherical symmetry.

In Fig. 10 we plot the mass aspect function at the outer boundary of the computational domain, $M(t, r_{max})$, as a function of time, and from four computations with grid spacings, Δr, in a 8:4:2:1 ratio. As was the case for the calculations discussed in the main text Sec. III, our convergence study uses a pulse of massless scalar field imploding onto a stable boson star So long as no scalar field (either real or complex) propagates off the computational grid, $M(t, r_{max})$ should be constant in time (and equal to the ADM mass), in the limit that $\Delta r \to 0$ (with $\Delta t \to 0$ implied since λ is always held fixed as Δr is varied).
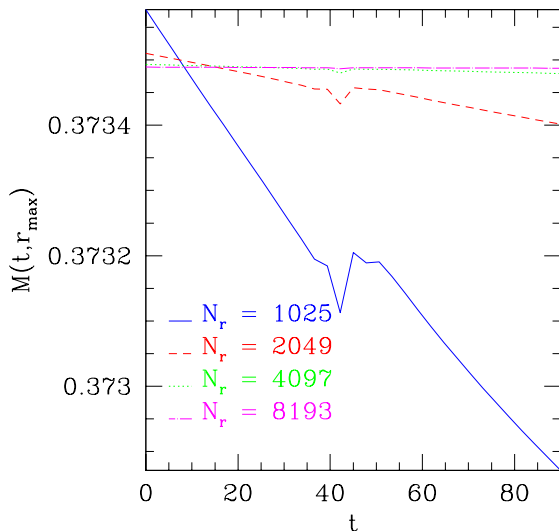
FIG. 10: Convergence test of the spherically symmetric code. The estimated ADM mass, $M(t, r_{\max})$, is plotted against time, t, for four calculations using numbers of spatial grid points, N_r, of $1025, 2049, 4097$ and 8193, so that the corresponding mesh spacings, Δr, are in a 8:4:2:1 ratio. The initial data parameters for the computations are: $\phi_0 = 0.01$ for the complex field, and $A_3 = 0.001, r_0 = 40$ and $\sigma = 3$ for the massless field (see (65)). The mass decreases with time in general, with a significant fluctuation at $40 \leq t \leq 50$, when the real scalar field is close to the origin and strongly interacts with the boson star. The variation in the computed total mass tends to vanish as we go to higher resolution. Combining results from the four calculations we find strong evidence that the finite difference scheme is second order accurate as expected.

In our test, the boson star has a central field value, $\phi_0 = 0.01$, while the incoming massless scalar field pulse is a gaussian of the form (65) with $A_3 = 0.001, r_0 = 40$ and $\sigma = 3$. The outer boundary is $r_{\max} = 300$, and we compute with $N_r = 1025, 2049, 4097$ and 8193. During the time interval $40 \leq t \leq 50$, the real scalar field is concentrated near the origin and interacts most strongly with the complex field. This results in a localized fluctuation of the computed ADM mass that is evident in the plots. However, $M(t, r_{\max})$ clearly tends to a constant value as the resolution is increased. In addition, from the differences of $M(t, r_{\max})$ computed at different resolutions (e.g. $M^{\Delta r}(t, r_{\max}) - M^{2\Delta r}(t, r_{\max})$, $M^{2\Delta r}(t, r_{\max}) - M^{4\Delta r}(t, r_{\max})$, etc.), we find strong evidence that the overall difference scheme is converging in a second order fashion.

[1] S. H. Hawley. PhD thesis, The University of Texas at Austin, unpublished, (2000).

[2] S. H. Hawley and M. W. Choptuik. *Phys. Rev.*, **D62**:104024, (2000).

[3] M. W. Choptuik. *Phys. Rev. Lett.*, **70**:9, (1993).

[4] C. Gundlach. *Phys. Rep.*, **376**:339–405, (2003).

[5] S. H. Hawley. Private communication (2003).

[6] R. Arnowitt, S. Deser, and C. W. Misner. In L. Witten, editor, *Gravitation: An Introduction to Current Research*. New York, Wiley, (1962).

[7] J. W. York, Jr. In L. Smarr, editor, *Sources of Gravitational Radiation*. Seattle, Cambridge University Press, (1979).

[8] C. W. Lai. *A Numerical Study of Boson Stars*. PhD thesis, The University of British Columbia, unpublished, (2004).

[9] R. Friedberg, T.D. Lee, and Y. Pang. *Phys. Rev.*, **D35**:3640–57, (1987).

[10] D. J. Kaup. *Phys. Rev.*, **172**:1331, (1968).

[11] W. H. Press et al. *Numerical recipes in FORTRAN : the art of scientific computing.* Cambridge University Press, (1992).

[12] J. Ventrella. *A Numerical Treatment of Spin-$\frac{1}{2}$ Fields Coupled to Gravity.* PhD thesis, The University of Texas at Austin, unpublished, (2002).

[13] R. D'Inverno. *Introducing Einstein's Relativity.* Oxford University Press, New York, (1992).

[14] A. P. Lightman et al. *Problem Book in Relativity and Gravitation.* Princeton University Press, (1975). Problem 15.3.

[15] M. Gleiser and R. Watkins. *Nucl. Phys.*, **B319**:733, (1989).

[16] H. Kreiss and J. Oliger. Methods for the approximate solution of time dependent problems. *Global Atmospheric Research Programme*, Publications Series No. **10**, (1973).